JOURNAL OF MATERIALS SCIENCE **36** (2001) 1585–1594

Fracture and deformation behaviour of melt growth composites at very high temperatures

Y. WAKU*
Japan Ultra-high Temperature Materials Research Institute, Ube City, Yamaguchi, 755-0001, Japan
E-mail: waku@jutem.co.jp

N. NAKAGAWA, H. OHTSUBO
Ube Research Laboratory, Corporate and Development, UBE Industries, Ltd., Ube City, Yamaguchi, 755-8633, Japan

A. MITANI, K. SHIMIZU
Japan Ultra-high Temperature Materials Research Institute, Ube City, Yamaguchi, 755-0001, Japan

Unidirectionally solidified $Al_2O_3/Y_3Al_5O_{12}$ (YAG) or $Al_2O_3/Er_3Al_5O_{12}$ (EAG) eutectic composites, which are named as Melt Growth Composites (MGCs) has recently been fabricated by unidirectional solidification. The MGCs have a new microstructure, in which continuous networks of single-crystal Al_2O_3 phases and single-crystal oxide compounds (YAG or EAG) interpenetrate without grain boundaries. The MGCs fabricated are thermally stable and has the following properties: 1) the flexural strength at room temperature can be maintained up to 2073 K (just below its melting point), 2) a fracture manner from room temperature to 2073 K is an intergranular fracture different from a transgranular fracture of sintered composite with the same composition, 3) the compressive creep strength at 1873 K and a strain rate of 10^{-4}/sec is 7–13 times higher than that of sintered composites, 4) the mechanism of creep deformation is based on the dislocation creep models completely different from the Nabarro-Herring or Coble creep models of the sintered composites, and 5) it shows neither weight gain nor grain growth, even upon heating at 1973 K in an air atmosphere for 1000 hours. The above superior high-temperature characteristics are caused by such factor as the MGCs having a single-crystal Al_2O_3/single-cryatal oxide compounds without grain boundaries and colonies, and the formation of the thermodynamically stable and compatible interface without amorphous phase.

1. Introduction

In the advanced gas generator field, studies all over the world are seeking to develop ultra-high-temperature structural materials that will improve thermal efficiency in aircraft engines and other high-efficiency gas turbines. A 1%-improvement of thermal efficiency would lead to a world-wide annual saving in energy costs of around $1000 billion [1], and research is being vigorously pursued into the development of very high temperature structural materials that remain stable under use for prolonged periods in an oxidizing atmosphere at very high temperatures.

Ceramics and ceramic-matrix-composites hold promise as structural materials with excellent heat resistance, oxidation resistance, and abrasion resistance and are therefore being examined and developed on a global scale. For example, to improve the combustion efficiency of gas turbines, operating temperatures must be increased and to achieve this, the development of ultra-high-temperature resistant structural materials is indispensable. Currently Ni-base superalloys are the main thrust in this field, but these have melting points of less than 1,673 K, and their strength deteriorates sharply in the region of 1,273 K. For this reason, in recent years to overcome the heat resistance limitations of metals, the development of turbine technology using advanced materials, centered on ceramic composites, has been vigorously pursued.

However, the strength of nearly all ceramic polycrystalline materials drops off rapidly with increases in temperature. According to Hillig [2], the strength in brittle materials should decrease proportionally to $(T/\mathrm{Tm})^{3/2}$, where T_m is the melting temperature. At 0.5 Tm, the strength is around half that at room temperature

* Author to whom all correspondence should be addressed.

because at high temperature, diffusional processes and grain boundaries, which lead to plastic deformation, play a large role [3].

D. Viechnicki *et al.* [4] conducted microstructural studies on an Al_2O_3/YAG system grown by the Bridgman method, and showed that the microstructure of the composite could be controlled by unidirectional solidification. In addition, it has recently been reported that a unidirectionally solidified Al_2O_3/YAG eutectic composite has superior flexural strength, thermal stability and creep resistance at high temperature [5–7], and is a candidate for high-temperature structural materials. However, since the composite consists of many eutectic colonies, a fairly strong influence of colony boundaries may be predicted [8].

On the other hand, Waku *et al.* [9–13] have recently fabricated MGCs consisting of a single crystal Al_2O_3 and single crystal oxide compounds such as YAG or EAG with neither colonies nor grain boundaries, using a unidirectional solidification method. In this paper, fracture and deformation behaviour of MGCs at very high temperatures is reported and discussed.

2. Experimental

2.1. Manufacturing of raw powder

Using commercially available Al_2O_3 powder (AKP-30, produced by Sumitomo Chemical Co., Ltd.), Y_2O_3 powder (Y_2O_3-RU, submicron-type, produced by Shin-Etsu Chemical Co., Ltd.) and Er_2O_3 powder (Er_2O_3-RU, submicron type, produced by Shin-Etsu Chemical Co., Ltd.), wet ball milling of $Al_2O_3/Y_2O_3 = 82/18$ or $Al_2O_3/Er_2O_3 = 81/19$ mol ratio was undertaken to obtain the uniform composite powder slurry. After removing the ethanol and drying the slurry using a rotary

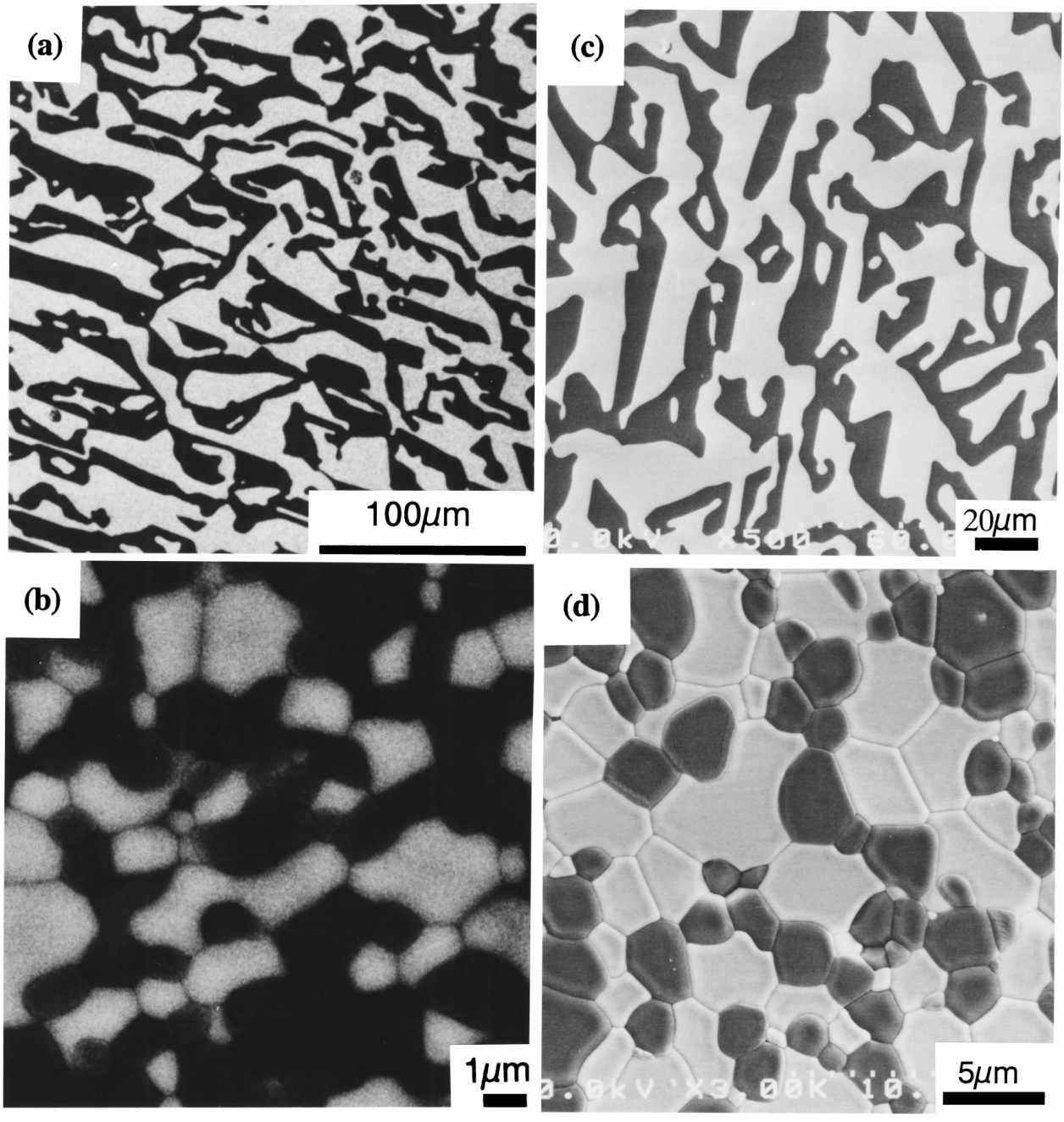

Figure 1 SEM images showing the microstructure of a cross-section perpendicular to the solidification direction of the MGCs ((a) and (c)) and parallel to the hot-pressed plane of the sintered composites ((c) and (d)). (a) and (b) for Al_2O_3/YAG system, (c) and (d) for Al_2O_3/EAG system.

evaporator, high-frequency induction heating to a Mo crucible (50 mm in diameter by 200 mm in length by 5 mm in thickness) was applied to perform preliminary melting and obtain ingots.

2.2. Unidirectional solidification

All experiments were performed using the Bridgman-type equipment at the Japan Ultra-high Temperature Materials Research Center. The ingot obtained by preliminary melting was inserted into Mo crucible (50 mm in outside diameter by 200 mm in length by 5 mm in thickness) placed in a vacuum chamber, and a graphite susceptor was heated by high-frequency induction heating. This heated the Mo crucible and facilitated the melting. After sustaining the melt of 2223 K (about 100 K above melting point) for 30 minutes, the Mo crucible was lowered at 5 mm an hour, completing the unidirectional solidification experiment.

2.3. Sintering

Mixed powders obtained using ball milling were hot-pressed in a carbon die to fabricate composite of $50 \times 70 \times 5$ mm at 1973 K under a 50 MPa pressure for an hour in a vacuum (10^{-2} mm Hg).

2.4. Evaluation process

The specimens used for three-point flexural were selected so that their axial direction was parallel to the direction of the unidirectional solidification. The dimensions of the flexural test specimen were $3 \times 4 \times 36$ mm with a 30-mm span. The three-point flexural strength was measured from room temperature to 2073 K in an argon atmosphere at a crosshead speed of 0.5 mm/min. The tests were carried out using the high-temperature uniaxial tension-compression and flexural test system (modified creep and fatigue machine, type 8562 produced by Instron) at the Japan Ultra-high Temperature Materials Research Center.

The specimens used in the compression creep test were also selected so that its axial direction was parallel to the solidification direction. Strain rate control compressive creep tests were carried out on the $4 \times 4 \times 6$ mm specimens. The specimen was heated by heating the carbon susceptor using high-frequency induction heating. The test temperatures were 1773 K, 1873 K, and 1973 K. The strain rates were 10^{-4}/sec, 10^{-5}/sec, and 10^{-6}/sec. The tests were conducted in an argon atmosphere. The equipment used in the tests was the same machine for flexural tests.

The oxidation resistance tests were carried out using a $6 \times 6 \times 6$ mm specimen. After holding the specimen for a fixed period at 1973 K in an air atmosphere, the specimen was tested for changes in its mass. Flexural test samples ($3 \times 4 \times 36$ mm) were also heated at 1973 K in an air atmosphere for a prescribed period. The flexural strength of these specimens was measured both at room temperature and at 1973 K following exposure. For a comparison, commercially available sintered SiC and Si_3N_4 were subjected to the same tests and measurement.

The thermal stability of the microstructure of the composite fabricated was evaluated from microstructural changes after heat treatment in an air atmosphere at 1973 K for up to 1000 hours using electric furnace with kanthal super 1900 heater.

Microstructural characterization was performed using the RAD-RB-type X-ray diffraction equipment produced by Rigaku Denki. High-resolution transmission microscopic (HRTEM) observation of the interface of the Al_2O_3 and the YAG phases was carried out using a JEM-2010 produced by Japan Electron, while the EPMA analysis was conducted with a JMX-8621MX by Japan Electron.

3. Results and discussion

3.1. Microstructures

Fig. 1 shows SEM images of the microstructure of a cross-section perpendicular to the solidification direction of an Al_2O_3/YAG ($Y_3Al_5O_{12}$) MGC and an Al_2O_3/EAG ($Er_3Al_5O_{12}$) MGC, and those of the hot-pressed plane of the sintered composite with the same composition as MGCs. For an Al_2O_3/YAG system ((a) and (b)), the light area in the SEM microstructure is

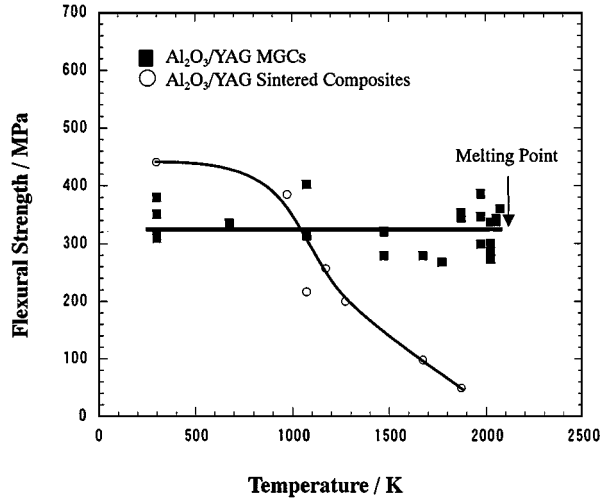

Figure 2 Temperature dependence of flexural strength of Al_2O_3/YAG MGCs compared with Al_2O_3/YAG sintered composites.

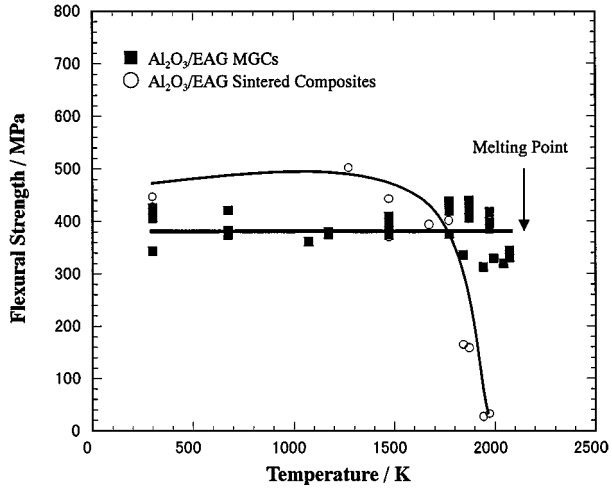

Figure 3 Temperature dependence of flexural strength of Al_2O_3/EAG MGCs compared with Al_2O_3/EAG sintered composites.

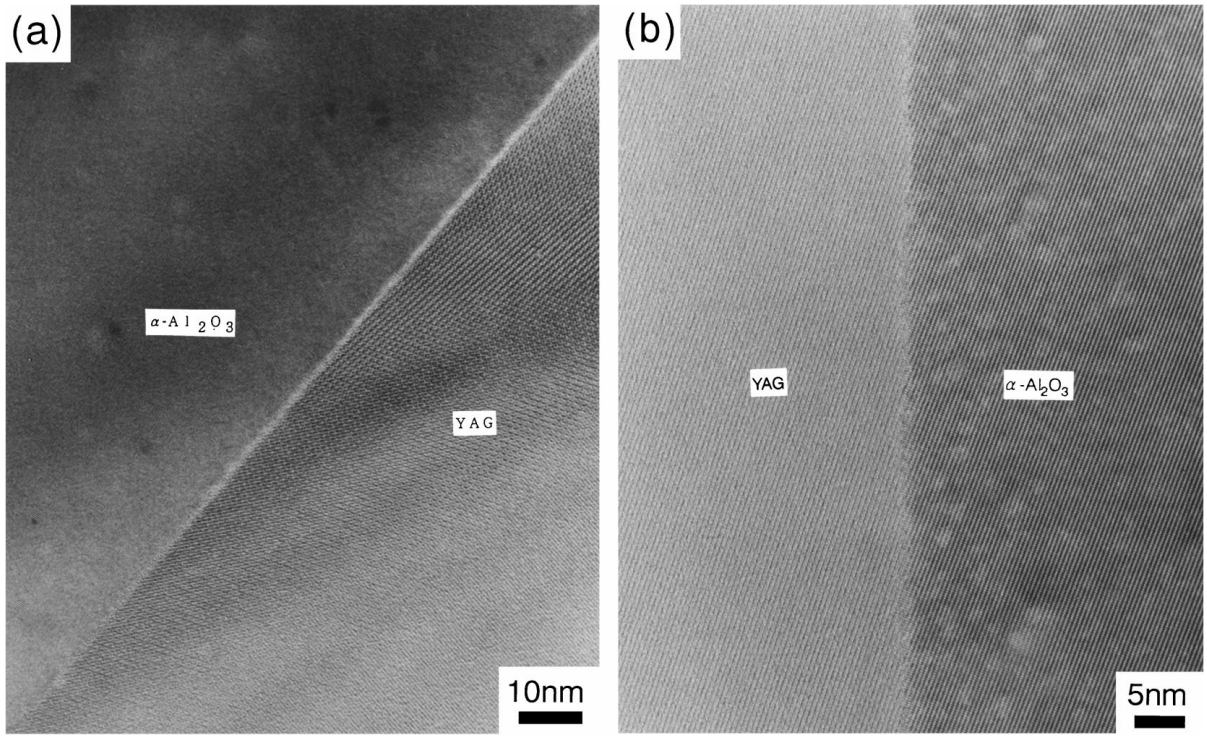

Figure 4 High-resolution TEM images of (a) the grain boundary between the Al_2O_3 and YAG phases in an Al_2O_3/YAG sintered composite and (b) the interface between Al_2O_3 and YAG phases of an Al_2O_3/YAG MGC.

the YAG phase, and the dark area is the Al_2O_3 phase (identified by EPMA analysis), the dimensions of the microstructures are 20–30 μm (this dimension is defined as the typical length to the short axis of each domain seen in the cross-section perpendicular to the solidification direction) for the MGC and 3–5 μm for the sintered composite. Homogeneous microstructures with no pores or colonies are observed in the MGC. The Al_2O_3/YAG MGCs consists of ⟨743⟩ single-crystal YAG with a garnet structure and ⟨110⟩ single-crystal Al_2O_3 with a hexagonal structure (from X-ray analysis). In contract, the sintered composite is a polycrystalline ceramic composite with random crystal orientations.

For an Al_2O_3/EAG system ((c) and (d)), both a MGC and a sintered composite consist of Al_2O_3 phases with a hexagonal structure and EAG phases with a garnet structure. The microstructure of the Al_2O_3/EAG MGC consists of single-crystal like Al_2O_3 phase and ⟨420⟩ single-crystal EAG phase with no colony or porosity. Unlike that, the sintered composite is a polycrystalline ceramic composite from the X-ray analysis. In the SEM microstructure ((c) and (d)), the white area is the EAG phase, the dark area is the Al_2O_3 phase from EPMA analysis. The dimensions of the microstructure of Al_2O_3/EAG MGCs are around 20–30 μm larger than that of around 3–5 μm for the sintered composites, as in an Al_2O_3/YAG system.

3.2. Temperature dependence of flexural strength

Figs 2 and 3 show the temperature dependence of the flexural strength of Al_2O_3/YAG MGCs and Al_2O_3/EAG MGCs from room temperature to 2073 K in comparison with that of a sintered composite of the same composition. Both MGCs maintain its room temperature strength up to 2073 K (just below its melting point of around 2100 K for an Al_2O_3/YAG MGCs and around 2130 K for Al_2O_3/EAG MGCs), with a flexural strength in the range of 300–400 MPa. In contrast, sintered composites has the same or higher flexural strength at room temperature, but its strength falls precipitously above 1073 K for an Al_2O_3/YAG sintered composites (Fig. 2) and above 1500 K for Al_2O_3/EAG sintered composites (Fig. 3).

The existence of amorphous phases at interfaces or grain boundaries generally leads to a reduction in the strength of the materials at high temperature [14, 15]. Fig. 4 shows typical high-resolution TEM images of the boundaries between Al_2O_3 and YAG phases in the sintered composite, and in the MGC. Amorphous phases are observed at the grain boundary of the sintered composite and also at the triple-grain junctions, grain boundaries between Al_2O_3 phases and between YAG phases in the sintered composite; but for the MGCs, no amorphous phases are observed at the interfaces between the Al_2O_3 and YAG phases and relatively compatible interfaces are formed. For an Al_2O_3/EAG system, according to the high-resolution TEM observation of the boundary between Al_2O_3 and EAG phases, similar results as the Al_2O_3/EAG MGCs are also observed [13].

Fig. 5 shows a SEM image of the fracture surface of an Al_2O_3/YAG MGC and an Al_2O_3/YAG sintered composite. Sintered composites show intergranular fracture at room temperature and at 1673 K and evidence for grain growth is clear. On the other hand, the Al_2O_3/YAG MGCs show no grain growth up to the very high temperature of 1973 K, and fracture is transgranular. Moreover, as shown in Fig. 5d, when the test temperature

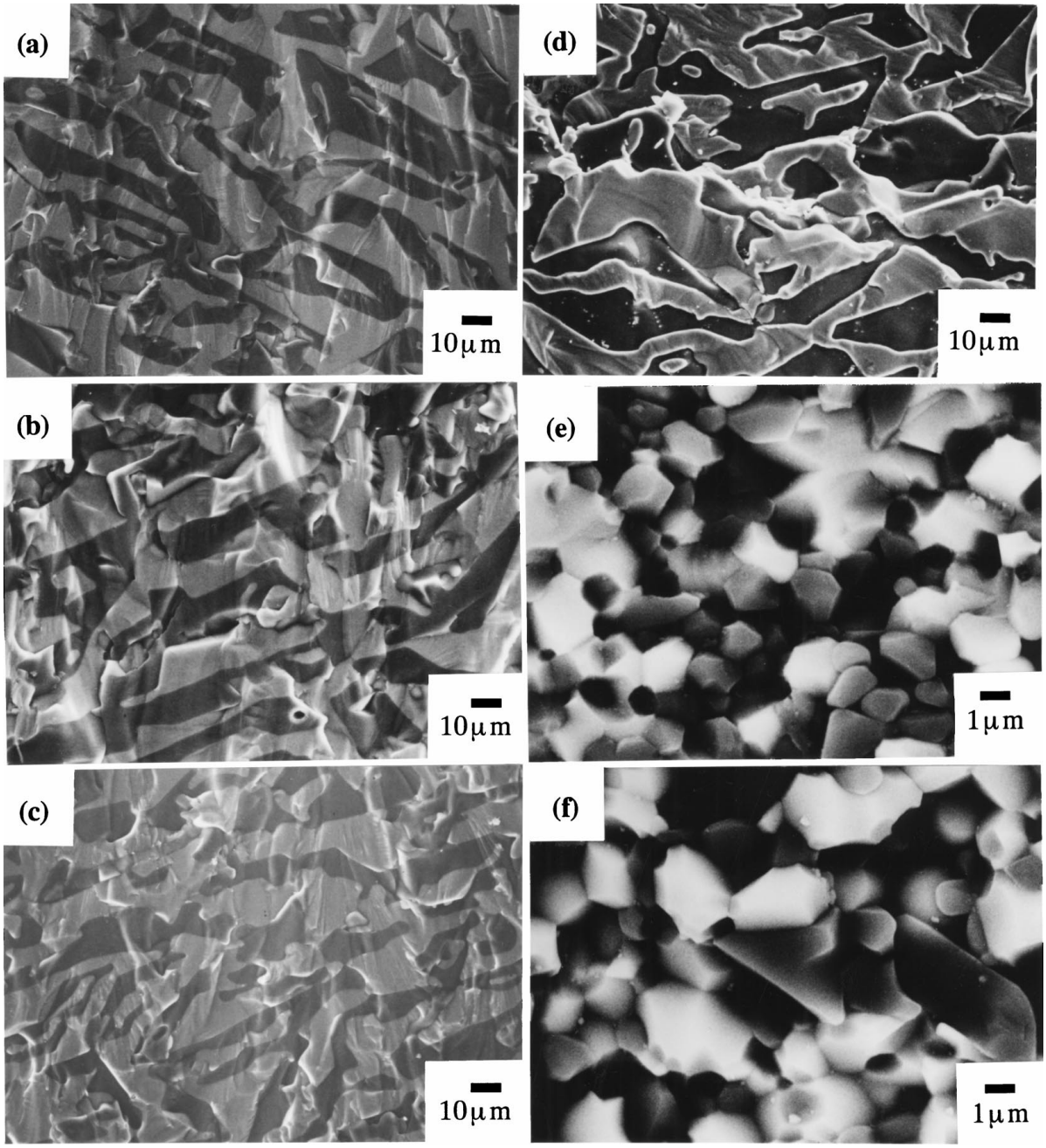

Figure 5 SEM photographs showing fracture surfaces in flexural specimens. For an Al_2O_3/YAG MGC: (a) at room temperature, (b) at 1673 K, (c) at 1973 K and (d) at 2073 K. For an Al_2O_3/YAG sintered composite: (d) at room temperature and (f) at 1673 K.

reaches 2073 K, fracture of the interface between Al_2O_3 and YAG phases and mixed fracture of intergranular and transgranular is observed. In the case of an Al_2O_3/EAG system, the almost same results as above mentioned are observed by SEM observation of fracture surfaces. Namely, a fracture manner of MGCs from room temperature to 2073 K is intergranular fracture completely different from transgranular fracture of sintered composites from room temperature to 1673 K.

Fig. 6 shows a SEM micrograph which illustrates the three-dimensional configuration of single-crystal YAG (Fig. 6a), single-crystal EAG phase (Fig. 6b) in the MGCs, and polycrystalline EAG phases (Fig. 6c) in the sintered composite, from which Al_2O_3 have been removed by heat treating in graphite powders at 1923 K for 2 hours. The configuration of single-crystal YAG and single-crystal EAG phases in the MGCs is a three-dimensionally connected porous structure, of shape is irregular. It is completely different from that of polycrystalline EAG phases including grain boundaries in the sintered composite. We therefore conclude that the present MGC has a microstructure in which continuous networks of single-crystal Al_2O_3 and single-crystal complex compound interpenetrate without grain boundaries.

3.3. Creep characteristics

Figs 7 and 8 show the relationship between compressive flow stress and strain rate in an Al_2O_3/YAG MGC and an Al_2O_3/EAG MGC at test temperatures of 1773 K, 1873 K and 1973 K and a sintered composite at 1873 K. The MGC and the sintered composite shared the same chemical composition, but their creep characteristics were markedly different. That is,

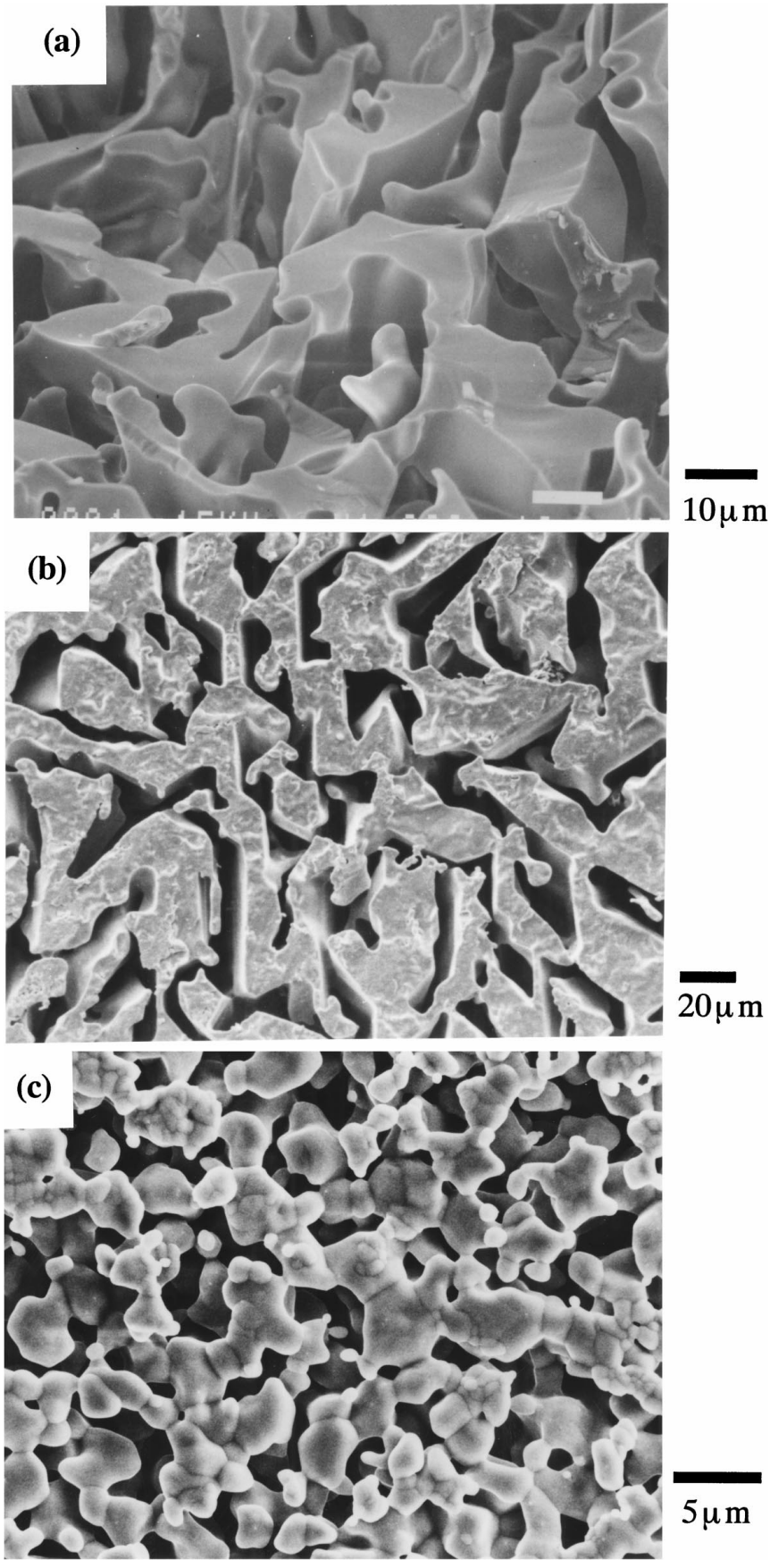

Figure 6 SEM micrographs showing the configuration of single-crystal YAG and single-crystal EAG phases in the MGCs, and polycrystalline EAG phases in the sintered composite. (a) single-crystal YAG phase, (b) single-crystal EAG phase, and (c) polycrystalline EAG phases.

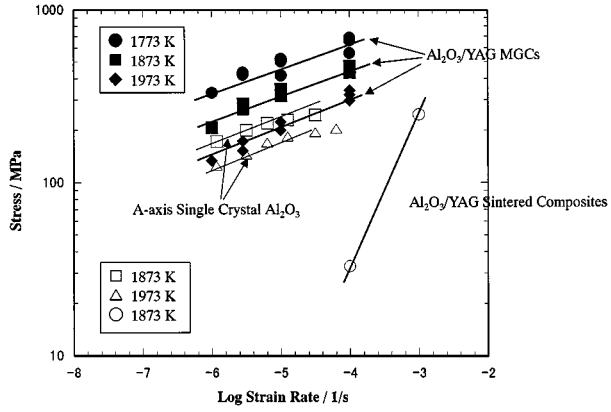

Figure 7 Comparison of compression creep in Al_2O_3/YAG MGCs and Al_2O_3 YAG sintered composites.

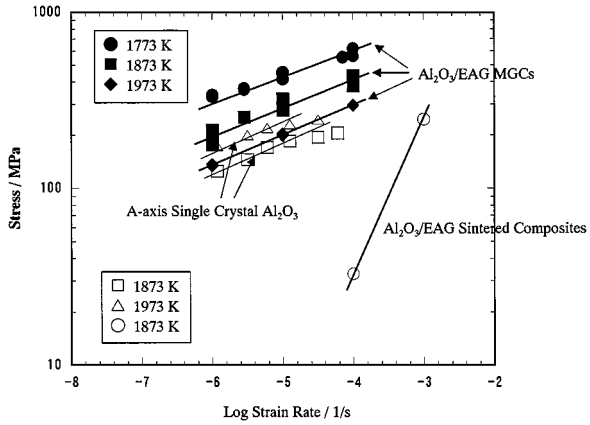

Figure 8 Comparison of compression creep in Al_2O_3/EAG MGCs and Al_2O_3/EAG sintered composites.

in the case of an Al_2O_3/YAG MGC, at the same strain rate of 10^{-4}/sec and test temperature of 1673 K, the sintered composite showed a creep stress of 33 MPa nearly same as polycrystalline YAG [16]. While the MGC's creep stress was approximately 13 times higher at 433 MPa. For an Al_2O_3/EAG system, as can be seen in Fig. 8, an Al_2O_3/EAG MGC showed a creep stress of 431 MPa around 8 times higher than that of 50 MPa for an Al_2O_3/EAG sintered composite at 10^{-4}/sec and at 1873 K. Moreover, as can be seen from Figs. 7 and 8, the MGC has creep characteristics that surpass those of *a*-axis sapphire fibers [17] and, as a bulk material, display excellent creep resistance.

Figs 9 and 10 show the bright field TEM images of dislocation structure for an Al_2O_3/YAG MGC and an a sintered composite (Fig. 9), and for an Al_2O_3/EAG MGC and a sintered composite (Fig. 10) observed in the specimens plastically deformed around 14% in the compressive test at an initial strain rate of 10^-5/sec and test temperature of 1873 K. Dislocation structure is observed in both Al_2O_3 phase and YAG phase for the Al_2O_3/YAG MGC, and in both Al_2O_3 phase and EAG phase for the Al_2O_3/EAG MGC, showing that the plastic deformation occurred by dislocation motion. While dislocation was not observed in both Al_2O_3 phase and YAG phase for the Al_2O_3/YAG sintered composite, and in both Al_2O_3 phase and EAG phase for the Al_2O_3/EAG sintered composite. The dislocation structures observed in both MGCs also indicate that the plastic deformation mechanism of the present MGC is essentially different from that of the sintered composite similar to the micrograin superplasticity of ceramics [18] due to a grain-boundary sliding or a liquid phase present at grain boundary at a high temperature.

The steady state creep rate $\dot{\varepsilon}$, can be usually shown by the following equation:

$$\dot{\varepsilon} = A\sigma^n \exp(-Q/RT) \tag{1}$$

Here, A and n are dimensionless coefficients, σ is the creep stress, Q is the activation energy for the creep, T is the absolute temperature, while R is the gas constant [19]. In Figs 7 and 8, the value of n is around 1–2 for Al_2O_3/YAG and Al_2O_3/EAG sintered composites, and 5–6 for Al_2O_3/YAG and Al_2O_3/EAG MGCs. In both sintered composites, it can be assumed that the creep deformation mechanism follows the Nabarro-Herring or Coble creep models, while in MGCs, the creep

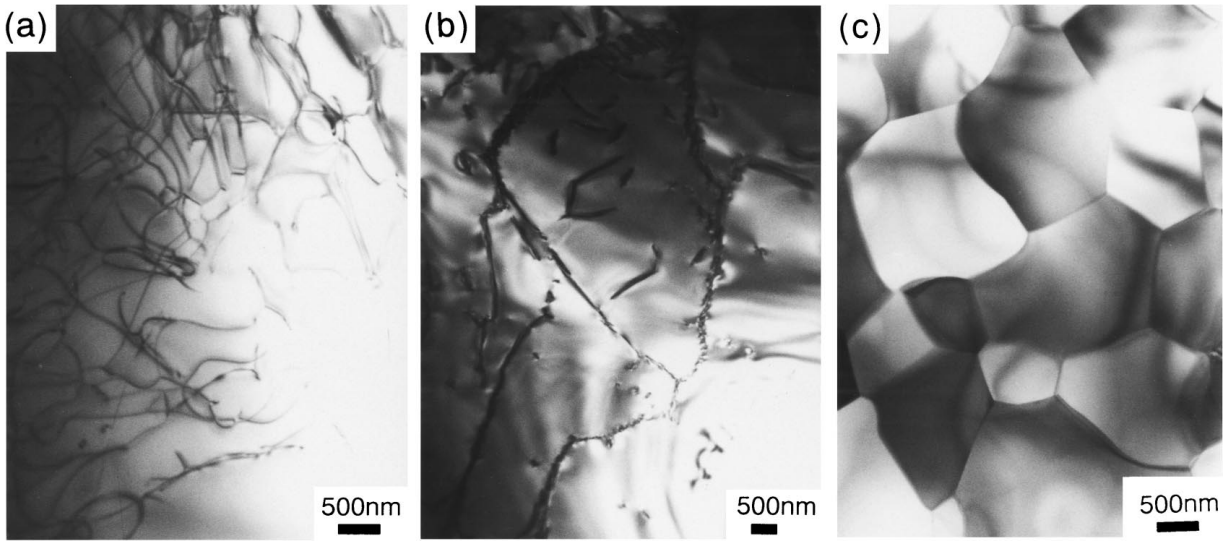

Figure 9 TEM images showing the dislocation structure of (a) Al_2O_3 phases and (b) YAG phases in the Al_2O_3/YAG MGC, and (c) the microstructure of Al_2O_3 and YAG phases in the sintered composites, of compressively crept specimens at 1873 K and strain rate of 10^{-5}/s.

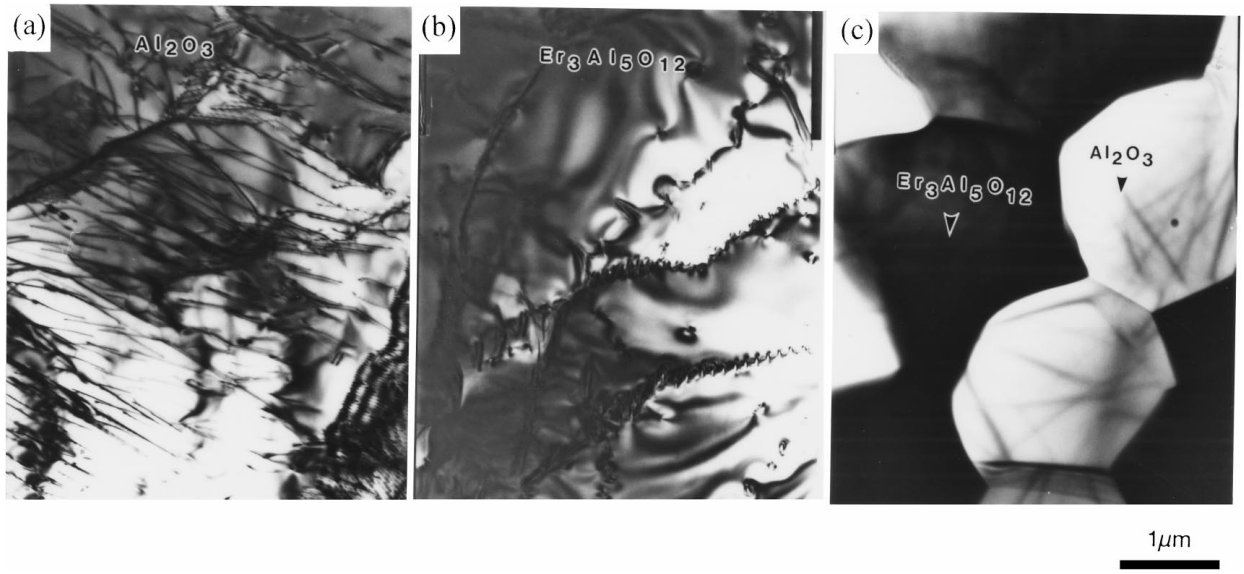

Figure 10 TEM images showing the dislocation structure of (a) Al_2O_3 phases and (b) EAG phases in the Al_2O_3/EAG MGC, and (c) the microstructure of Al_2O_3 and EAG phases in the sintered composites, of compressively crept specimens at 1873 K and strain rate of 10^{-5}/s.

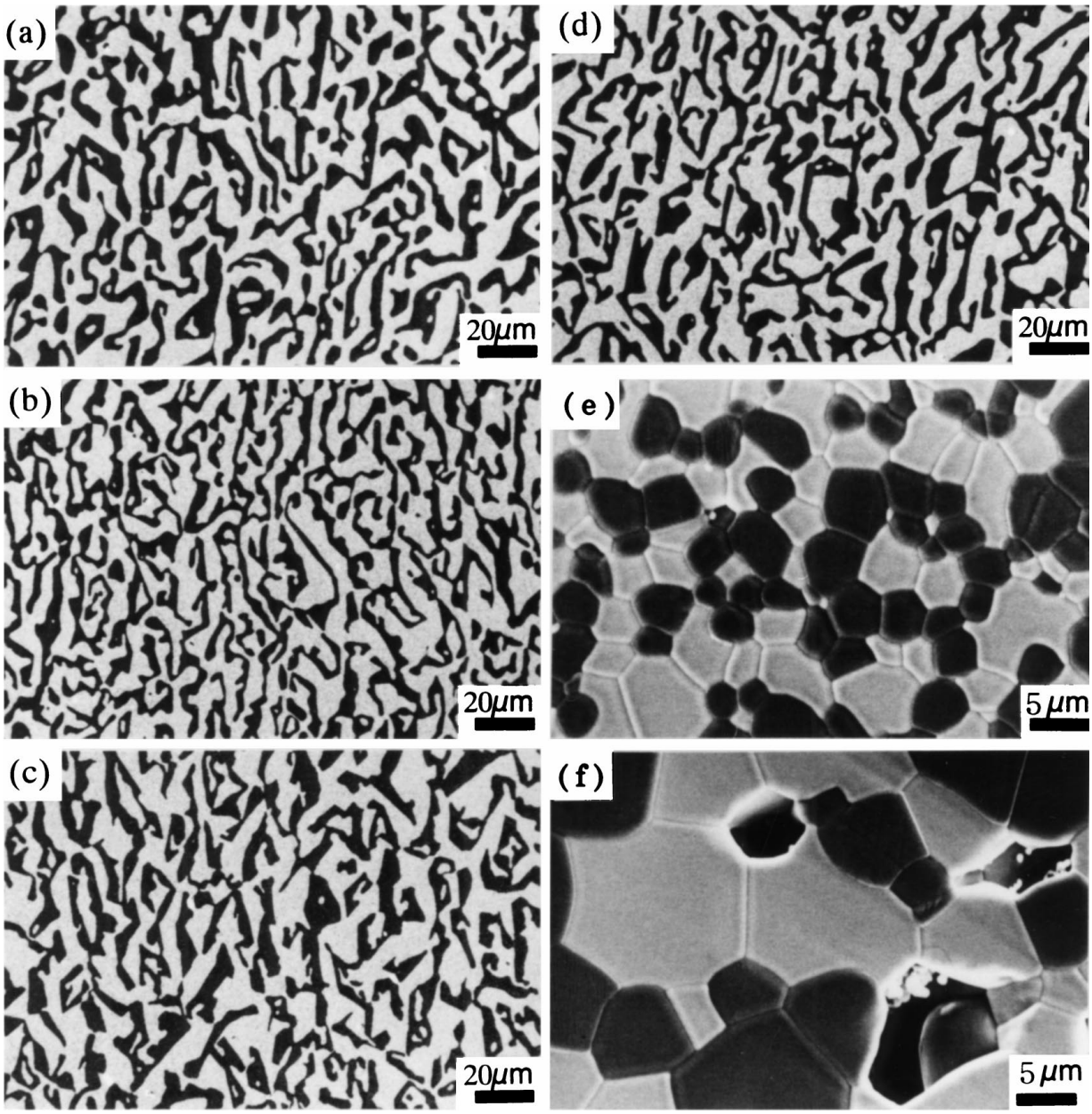

Figure 11 SEM images showing thermal stability of the microstructures at 1973 K in an air atmosphere in Al_2O_3/EAG MGCs: (a) as-received, after heat treatment for (b) 500 h, (c) 750 h, (d) 1000 h and Al_2O_3/EAG sintered composites: (e) as-received and after heat treatment for (f) 100 h.

deformation mechanism can be assumed to follow the dislocation creep models corresponding to the dislocation structure in Figs 9 and 10. The activation energy Q is estimated to be about 730 kJ/mol from an Arrhenius plot [20], which is not so different from the values estimated from the high temperature creep in Al_2O_3 single crystal (compression axis is [110]) and YAG single crystal (compression axis is [110]) [16, 21, 22]. It is also reported that the activation energy for oxygen diffusion in Al_2O_3 is about 665 kJ/mol [22], which is not so far from the activation energy of Al_2O_3 single crystal for plastic flow even though that of Al^+ diffusion is about 476 kJ/mol [23]. This fact means that the deformation mechanism of the Al_2O_3 single crystal is the diffusion controlled dislocation creep. On the other hand, the activation energy for oxygen diffusion in YAG is about 310 kJ/mol [24, 25], which differs significantly from the activation energy of YAG single crystal for plastic flow. However, dislocation is always observed in both Al_2O_3 phase and YAG phase of compressively deformed specimens at 1773 K–1973 K and at strain rate of 10^{-4}/s–10^{-6}/s. Therefore, the compressive deformation mechanism of the Al_2O_3/YAG MGC must follow the dislocation creep models. In case of Al_2O_3/EAG MGCs, there are no data on diffusion and creep, so we cannot discuss in detail. However, from Figs 8 and 10, it can be presumed that the compressive deformation mechanism of Al_2O_3/EAG MGC is the almost same as Al_2O_3/YAG MGCs.

3.4. Oxidation resistance and thermal stability

Al_2O_3/YAG and Al_2O_3/EAG MGCs have excellent oxidation resistance with no change in mass gain for 1000 hour at 1973 K in an air atmosphere [11, 12]. There were also no changes in flexural strength both at room temperature and 1973 K even after heat treatment for 1000 hours at 1973 K in an air atmosphere. In contrast, when Si_3N_4 advanced ceramic was exposed to 1973 K for 10 hours in the atmosphere, the collapse of the shape occurred. Likewise, when SiC was held at 1973 K for 50 hours, it was also shown to be unstable owing to the collapse of the shape also occurred.

Fig. 11 shows SEM images of the microstructure of an Al_2O_3/EAG MGC after 500, 750 and 1000 hours of heat treatment at 1973 K in an air atmosphere. Even after 1000 hours of heat treatment no grain growth of microstructure was observed. The MGCs were shown to be very stable during lengthy exposure at high temperature of 1973 K in an air atmosphere. This stability resulted from the thermodynamic stability at that temperature of the constituent phases of the single-crystal like Al_2O_3 and the single- crystal EAG, and the thermodynamic stability of the interface. In contrast, a sintered composite shows grain growth and there are many pores lead to reduction of strength at 1973 K only for 100 hr [13].

4. Conclusions

The MGCs have superior high-temperature strength characteristics with flexural strength showing no temperature dependence in the range from room temperature up to 2073 K. The compressed creep resistance of the MGCs were 8–13 times higher than a sintered composite with the same chemical composition. While the stress exponent, n, for the sintered composites were 1–2, that for the MGCs were 5–6. The activation energy for the steady state creep of the MGC was around 730 kJ/mol. After 1000 hours at 1973 K in an air atmosphere no change whatsoever was observed in the highly stable eutectic composite's mass. The MGCs also have a very thermally stable microstructure with no grain growth in evidence after lengthy heat treatment at a high temperature of 1973 K in an air atmosphere.

These excellent high-temperature characteristics of the MGCs are closely linked to such factors as: (1) the MGC has a microstructure consisting of three-dimensionally continuous and complexly entangled single-crystal Al_2O_3 phase and single-crystal oxide compounds such as YAG or EAG phases without grain boundaries, (2) interfaces with thermodynamically stable and comparatively good coherency, and no amorphous phases are formed.

References

1. The Japan Industrial Journal **12** (1994) 6.
2. W. B. HILLIG, in "Tailoring Multiphase and Composite Ceramics," edited by R. E. Tressler, G. L. Messing, C. G. Pantano, and R. E. Newnham (Plenum Press, New York); *Materials Science Research* **20** (1986) 697.
3. E. L. COURTRIGHT, H. C. GRAHAM, A. P. KATZ and R. J. KERANS, "Ultrahigh temperature assessment study-ceramic matrix composites." (Materials Directorate, Wright Laboratory, Air Force Materiel Command, Wright-Patterson Air Force Base, 1992) p. 1.
4. D. VIECHNICKI and F. SCHMID, *J. Mater. Sci.* **4** (1969) 84.
5. T. MAH and T. A. PARTHASARATHY, *Ceram. Eng. Sci. Proc.* **11** (1990) 1617.
6. T. A. PARTHASARATHY, T. MAH and L. E. MATSON, *ibid.* **11** (1990) 1628.
7. T. A. PARTHASARATHY, M. TAI-II and L. E. MATSON, *J. Amer. Ceram. Sci.* **76** (1993) 29.
8. V. S. STUBICAN, R. C. BRADT, F. L. KENNARD, W. J. MINFORD and C. C. SORREL, in "Tailoring Multiphase and Composite Ceramics," edited by R. E. Tressler, G. L. Messing, C. G. Pantano, and R. E. Newnham (Plenum Press, New York); *Materials Science Research* **20** (1986) 697.
9. Y. WAKU, N. NAKAGAWA, H. OHTSUBO, Y. OHSORA and Y. KOHTOKU, *J. Japan Inst. Metals* **59** (1995) 71.
10. Y. WAKU, H. OTSUBO, N. NAKAGAWA and Y. KOHTOKU, *J. Mater. Sci.* **31** (1996) 4663.
11. Y. WAKU N. NAKAGAWA, T. WAKAMOTO, H. OHTSUBO, K. SHIMIZU and Y. KOHTOKU, *ibid.* **33** (1998) 1217.
12. *Idem., ibid.* **33** (1998) 4943.
13. N. NAKAGAWA, Y. WAKU, T. WAKAMOTO, H. OHTSUBO, K. SHIMIZU and Y. KOHTOKU, *J. Japan Inst. Metals* **64** (2000) 101.
14. D. R. CLARKE, *J. Amer. Ceram. Soc.* **62** (1979) 236.
15. J. ECHIGOYA, S. HAYASHI, K. SASAKI and H. SUTO, *J. Japan Inst. Metals* **48** (1984) 430.
16. T. A. PARTHASARATHY, T. MAH and K. KELLER, *J. Amer. Ceram. Soc.* **75** (1992) 1756.
17. D. M. KOTCHICK and R. E. TRESSLER, *ibid.* **63** (1980) 429.
18. F. WAKAI, Y. KODAMA, S. SAKAGUCHI, N. MURAYAMA, K. IZEKI and K. NIIHARA, *Nature* **344** (1990) 421.
19. W. R. CANNON and T. G. LAGDON, *J. Mater. Sci.* **18** (1983) 1.

20. H. YOSHIDA, K. SHIMURA, S. SUGINOHARA, Y. IKUHARA and T. SAKUMA, N. NAKAGAWA and Y. WAKU, in Proceeding of the 8th International Conference on Creep and Fracture of Engineering Materials and Structures, November 1–5, 1999 Tsukuba (2000) Vol. 171–174, p. 855.
21. S. KARATO, Z. WANG and K. FUJINO, *J. Mater. Sci.* **29** (1994) 6458.
22. G. S. CORMAN, *J. Mater. Sci. Lett.* **12** (1993) 379.
23. A. E. PALADINO and W. D. KINGERY, *J. Chem. Phys.* **37** (1962) 957.
24. J. D. FRECCH, J. ZHAO, M. P. HARMER, H. M. CHAN and G. A. MILLER, *J. Amer. Ceram. Soc.* **77** (1994) 2857.
25. H. HANADA, Y. MIYAZAWA and S. SHIRASAKI, *J. Cryst. Growth* **68** (1984) 581.

Received 24 July
and accepted 16 October 2000